Research Article | Vol. 25, No. 19 | 18 Sep 2017 | OPTICS EXPRESS 22667
Optics EXPRESS

Compensation-free broadband entangled photon pair sources

CHANGJIA CHEN,[1,*] ERIC Y. ZHU,[1] ARASH RIAZI,[1] ALEXEY V. GLADYSHEV,[2] COSTANTINO CORBARI,[3] MORTEN IBSEN,[3] PETER G. KAZANSKY,[3] AND LI QIAN[1,4]

[1]*Dept. of Electrical and Computer Engineering, University of Toronto, 10 King's College Rd., Toronto, ON M5S 3G4, Canada*
[2]*Fiber Optics Research Center, Russian Academy of Sciences, 38 Vavilov Street, 119333 Moscow, Russia*
[3]*Optoelectronics Research Centre, University of Southampton, Southampton SO17 1BJ, UK*
[4]*National Engineering Laboratory for Fiber Optic Sensor Technology, Wuhan University of Technology, Wuhan 430070, China*
[*]*changjia.chen@mail.utoronto.ca*

Abstract: Quantum sources that provide broadband biphotons entangled in both polarization and time-energy degrees of freedom are a rich quantum resource that finds many applications in quantum communication, sensing, and metrology. Creating such a source while maintaining high entanglement quality over a broad spectral range is a challenge, which conventionally requires various compensation steps to erase temporal, spectral, or spatial distinguishabilities. Here, we point out that in fact compensation is not always necessary. The key to generate broadband polarization-entangled biphotons via type-II spontaneous parametric downcoversion (SPDC) without compensation is to use nonlinear materials with sufficiently low group birefringence that the biphoton bandwidth becomes dispersion-limited. Most nonlinear crystals or waveguides cannot meet this condition, but it is easily met in fiber-based systems. We reveal the interplay of group birefringence and dispersion on SPDC bandwidth and polarization entanglement quality. We show that periodically poled silica fiber (PPSF) is an ideal medium to generate high-concurrence (>0.977) polarization-entangled photons over a broad spectral range (>77nm), directly and without compensation. This is the highest polarization-entanglement concurrence reported that is maintained over a broad spectral range from a compensation-free source.

OCIS codes: (270.0270) Quantum optics; (190.4370) Nonlinear optics, fibers.

References and links

1. R. Horodecki, P. Horodecki, M. Horodecki, and K. Horodecki, "Quantum entanglement," Rev. Mod. Phys. **81**(2), 865 (2009).
2. A. Fraine, D. Simon, O. Minaeva, R. Egorov, and A. Sergienko, "Precise evaluation of polarization mode dispersion by separation of even-and odd-order effects in quantum interferometry," Opt. Express **19**(23), 22820–22836 (2011).
3. A. F. Abouraddy, K. C. Toussaint Jr, A. V. Sergienko, B. E. Saleh, and M. C. Teich, "Entangled-photon ellipsometry," J. Opt. Soc. Am. B **19**, 656–662 (2002).
4. C. Xiong, X. Zhang, Z. Liu, M. Collins, A. Mahendra, L. Helt, M. Steel, D.-Y. Choi, C. Chae, P. Leong, B. J. Eggleton, "Active temporal multiplexing of indistinguishable heralded single photons," Nat. Commun. **7**, 10853 (2016).
5. B. Qi, "Single-photon continuous-variable quantum key distribution based on the energy-time uncertainty relation," Opt. Lett. **31**, 2795–2797 (2006).
6. C. Reimer, L. Caspani, M. Clerici, M. Ferrera, M. Kues, M. Peccianti, A. Pasquazi, L. Razzari, B. E. Little, S. T. Chu, D. J. Moss, and R. Morandotti, "Integrated frequency comb source of heralded single photons," Opt. Express **22**(6), 6535–6546 (2014).
7. T. Zhong, F. N. Wong, A. Restelli, and J. C. Bienfang, "Efficient single-spatial-mode periodically-poled ktiopo 4 waveguide source for high-dimensional entanglement-based quantum key distribution," Opt. Express **20**(24), 26868–26877 (2012).
8. P. G. Kwiat, "Hyper-entangled states," J. Mod. Opt. **44**, 2173–2184 (1997).
9. S. P. Walborn, "Hyperentanglement: Breaking the communication barrier," Nat. Phys. **4**, 268–269 (2008).
10. K. Mattle, H. Weinfurter, P. G. Kwiat, and A. Zeilinger, "Dense coding in experimental quantum communication," Phys. Rev. Lett. **76**(25), 4656 (1996).

#297259 https://doi.org/10.1364/OE.25.022667
Journal © 2017 Received 2 Jun 2017; revised 1 Sep 2017; accepted 1 Sep 2017; published 8 Sep 2017

Optics EXPRESS

11. S. Dong, L. Yu, W. Zhang, J. Wu, W. Zhang, L. You, and Y. Huang, "Generation of hyper-entanglement in polarization/energy-time and discrete-frequency/energytime in optical fibers," Sci. Rep. **5**, 9195 (2015).
12. E. Y. Zhu, C. Corbari, A. Gladyshev, P. Kazansky, H. Lo, and L. Qian, "Multi-party agile quantum key distribution network with a broadband fiber-based entangled source," https://arXiv:1506.03896 (2015).
13. H. C. Lim, A. Yoshizawa, H. Tsuchida, and K. Kikuchi, "Broadband source of telecom-band polarization-entangled photon-pairs for wavelength-multiplexed entanglement distribution," Opt. Express **16**(20), 16052–16057 (2008).
14. T. E. Keller and M. H. Rubin, "Theory of two-photon entanglement for spontaneous parametric down-conversion driven by a narrow pump pulse," Phys. Rev. A **56**(2), 1534 (1997).
15. H. C. Lim, A. Yoshizawa, H. Tsuchida, and K. Kikuchi, "Stable source of high quality telecom-band polarization entangled photon-pairs based on a single, pulse-pumped, short ppln waveguide," Opt. Express **16**(17), 12460–12468 (2008).
16. Y. H. Kim, M. V. Chekhova, S. P. Kulik, M. H. Rubin, and Y, Shih, "Interferometric Bell-state preparation using femtosecond-pulse-pumped spontaneous parametric down-conversion," Phys. Rev. A, **63**(6), 062301 (2001).
17. M. Fiorentino, M. Gaétan, CE Kuklewicz, FNC Wong, and J. H. Shapiro, "Generation of ultrabright tunable polarization entanglement without spatial, spectral, or temporal constraints," Phys. Rev. A **69**(4), 041801 (2004).
18. B. S. Shi, and A. Tomita, "Generation of a pulsed polarization entangled photon pair using a Sagnac interferometer," Phys. Rev. A **69**(1), 013803 (2004).
19. Y. Li, Z.Y. Zhou, D.S. Ding, and B.S. Shi, "CW-pumped telecom band polarization entangled photon pair generation in a Sagnac interferometer," Opt. Express, **23**(22), 28792–28800, (2015).
20. T. Kim, M. Fiorentino, and F. Wong, "Phase-stable source of polarization-entangled photons using a polarization Sagnac interferometer," Phys. Rev. A **73**(1), 012316 (2006).
21. G. Fujii, N. Namekata, M. Motoya, S. Kurimura, and S. Inoue, "Bright narrowband source of photon pairs at optical telecommunication wavelengths using a type-ii periodically poled lithium niobate waveguide," Opt. Express **15**(20), 12769–12776 (2007).
22. C. Kurtsiefer, M. Oberparleiter, and H. Weinfurter, "High efficiency entangled photon pair collection in type-ii parametric fluorescence," Phys. Rev. A **64**(2), 023802 (2001).
23. A. Fraine, O. Minaeva, D. Simon, R. Egorov, and A. Sergienko, "Broadband source of polarization entangled photons," Opt. Lett. **37**(11), 1910–1912 (2012).
24. E. Y. Zhu, Z. Tang, L. Qian, L. G. Helt, M. Liscidini, J. Sipe, C. Corbari, A. Canagasabey, M. Ibsen, and P. G. Kazansky, "Direct generation of polarization-entangled photon pairs in a poled fiber," Phys. Rev. Lett. **108**(21), 213902 (2012).
25. E. Y. Zhu, Z. Tang, L. Qian, L. Helt, M. Liscidini, J. Sipe, C. Corbari, A. Canagasabey, M. Ibsen, and P. Kazansky, "Poled-fiber source of broadband polarization-entangled photon pairs," Opt. Lett. **38**(21), 4397–4400 (2013).
26. T. S. Humble and W. P. Grice, "Spectral effects in quantum teleportation," Phys. Rev. A **75**, 022307 (2007).
27. L. G. Helt, M. Liscidini, and J. E. Sipe, "How does it scale? comparing quantum and classical nonlinear optical processes in integrated devices," J. Opt. Soc. Am. B **29**, 2199–2212 (2012).
28. A. Sergienko, Y. Shih, and M. Rubin, "Experimental evaluation of a two-photon wave packet in type-ii parametric downconversion," J. Opt. Soc. Am. B **12**, 859–862 (1995).
29. W. K. Wootters, "Entanglement of formation of an arbitrary state of two qubits," Phys. Rev. Let. **80**(10), 2245 (1998).
30. R. T. Horn, P. Kolenderski, D. Kang, P. Abolghasem, C. Scarcella, A. Della Frera, A. Tosi, L. G. Helt, S. V. Zhukovsky, J. E. Sipe, and G. Weihs, "Inherent polarization entanglement generated from a monolithic semiconductor chip," Sci. Rep. **3**, 2314 (2013).
31. K. Laiho, B. Pressl, A. Schlager, H. Suchomel, M. Kamp, S. Höfling, C. Schneider, and G. Weihs, "Uncovering dispersion properties in semiconductor waveguides to study photon-pair generation," Nanotechnology **27**, 434003 (2016).
32. D. E. Zelmon, D. L. Small, and D. Jundt, "Infrared corrected sellmeier coefficients for congruently grown lithium niobate and 5 mol.% magnesium oxide-doped lithium niobate," J. Opt. Soc. Am. B **14**, 3319–3322 (1997).
33. A. Martin, V. Cristofori, P. Aboussouan, H. Herrmann, W. Sohler, D. B. Ostrowsky, O. Alibart, and S. Tanzilli, "Integrated optical source of polarization entangled photons at 1310 nm," Opt. Express **17**(2), 1033–1041 (2009).
34. D. Zhang, Y. Kong, and J. Y. Zhang, "Optical parametric properties of 532-nm-pumped beta-barium-borate near the infrared absorption edge," Opt. Commun. **184**, 485–491 (2000).
35. A. Canagasabey, C. Corbari, Z. Zhang, P. G. Kazansky, and M. Ibsen, "Broadly tunable second-harmonic generation in periodically poled silica fibers," Opt. Lett. **32**(13), 1863–1865 (2007).
36. I. Malitson, "Interspecimen comparison of the refractive index of fused silica," J. Opt. Soc. Am. **55**, 1205–1209 (1965).
37. J. Fleming, "Material and mode dispersion in GeO_2.B_2O_3.SiC_2 glasses," J. Am. Cer. Soc. **59**, 503–507 (1976).
38. S. Kobayashi, T. Izawa, N. Shibata, and S. Shibata, "Characteristics of optical fibers in infrared wavelength region," Electron. Commun. Jap. **26**, 453–467 (1978).
39. E. Y. Zhu, C. Corbari, P. Kazansky, and L. Qian, "Selfcalibrating fiber spectrometer for the measurement of broadband downconverted photon pairs," https://arXiv:1505.01226 (2015).
40. A. Schlager, B. Pressl, K. Laiho, H. Suchomel, M. Kamp, S. Höfling, C. Schneider, and G. Weihs, "Temporally versatile polarization entanglement from Bragg reflection waveguides," Opt. Lett. **42**(11), 2102–2105 (2017).
41. M. V. Pack, D. J. Armstrong, and A. V. Smith, "Measurement of the $\chi(2)$ tensors of KTiOPO4, KTiOAsO4,

Optics EXPRESS

RbTiOPO4, and RbTiOAsO4 crystals," Appl. Opt., **43**(16), 3319–3323 (2004).
42. M. C. Teich, B. E. Saleh, F. N. Wong, and J. H. Shapiro, "Variations on the theme of quantum optical coherence tomography: a review," Quantum Info. Proc., **11**(4), 903–923.(2012).
43. J. M. Lukens, and P. Lougovski, "Frequency-encoded photonic qubits for scalable quantum information processing," Optica, **4**(1), 8–16 (2017).

1. Introduction

Entangled photons are a fundamental resource in many applications of quantum optics [1]. Broadband entanglement sources have been used in applications such as high-resolution [2] and spectrally-tunable [3] quantum interferometry and metrology. They have also been utilized in various schemes of quantum key distribution (QKD), either as a means of providing heralded single-photon sources [4–6] or as a source of time-energy entanglement for large-alphabet QKD [7]. Moreover, hyper entanglement [8], in which the quantum systems are entangled in multiple degrees of freedom such as polarization and energy-time, finds its utilization in an even wider spectrum of applications [8–11] . Recently, such entangled sources were also used in realizing a dynamically reconfigurable multi-user QKD [12, 13] networks.

Creating a broadband hyper-entangled source is challenging. Take, for example, SPDC, the most widely used technique for bipartite polarization entanglement generation. Type-0 or type-I SPDC produces photon pairs of the same polarization, and therefore cannot generate polarization entanglement directly. One would have to use two such processes to generate orthogonally polarized photon pairs separately, and then employ an additional interference step to remove which-way information [13–15], greatly increasing the system complexity. For example, Mach-Zehnder interferometers [16, 17] are very sensitive to alignment and environmental perturbation, such as temperature fluctuation. Hence it requires active servo control of a pump interferometer in order to set the phase of the biphoton state. Entanglement sources based upon Sagnac interferometers [18–20] are immune to perturbation, but have technical difficulties such as requiring triple wavelength polarization beamsplitters and dual wavelength half-wave plates. These challenges become even more difficult to solve for broadband polarization entanglement generation. In contrast, direct generation of polarization-entangled photons by type-II SPDC is simple and more desirable. However, type-II SPDC in nonlinear crystals is much narrower in bandwidth (typically<5nm) [21, 22] due to the difficulty in (1) sustaining phase matching and (2) erasing temporal and spectral distinguishability, over a broad bandwidth. Even when a chirped quasi-phase-matched (QPM) waveguide is used to satisfy phase-matching over a broad spectral range [23], temporal distinguishability brought by the large group birefringence still has to be compensated exactly, and spectral distinguishability still severely degrades the quality of polarization entanglement.

Is it possible to generate high-quality broadband polarization entanglement directly, *compensation-free*? Experimental demonstration of such a source in periodically poled silica fiber (PPSF) [24, 25] exists, but the fundamental criteria for such a source are missing. In this paper, we investigate the interplay of group birefringence and dispersion on temporal and spectral indistinguishability, and the condition under which both temporal and spectral distinguishabilities are negligibly small. We point out that, compensation-free broadband entanglement is only possible when dispersion, as opposed to group birefringence, becomes the limiting factor for SPDC bandwidth. Such a condition is rarely met in nonlinear crystals and waveguides due to their large group birefringence, but it is readily achievable in fiber. We experimentally demonstrate that broadband high quality polarization entanglement can be realized in a PPSF source.

2. Theory

To produce highly entangled biphotons both in polarization and time-energy degrees of freedom, we use type-II SPDC pumped by a narrowband continuous-wave (CW) or quasi-CW pump. This

Optics EXPRESS

is the condition we consider throughout the paper. The biphoton wavefunction expressed in the frequency domain then becomes [26]:

$$|\Psi\rangle = \frac{1}{\sqrt{2}} \int \mathrm{d}\omega_s \int \mathrm{d}\omega_i (f_-(\omega_s, \omega_i)(|H, \omega_s\rangle\, |V, \omega_i\rangle + f_+(\omega_s, \omega_i)\, |V, \omega_s\rangle\, |H, \omega_i\rangle). \tag{1}$$

Ideally in the generation of Bell state $|\Psi^+\rangle$, f_- and f_+ should be identical. However, the state generated via type-II SPDC is not exacly $|\Psi^+\rangle$ due to the anisotropy of nonlinear medium. The f_- and f_+ function are given by:

$$\begin{cases} f_-(\omega_s, \omega_i) \propto \exp\left[i\dfrac{(\beta_H^{\omega_s} + \beta_V^{\omega_i})L}{2}\right] \times \mathrm{sinc}\left(\dfrac{L}{2}\Delta\beta_{f_-}\right) \\ f_+(\omega_s, \omega_i) \propto \exp\left[i\dfrac{(\beta_H^{\omega_i} + \beta_V^{\omega_s})L}{2}\right] \times \mathrm{sinc}\left(\dfrac{L}{2}\Delta\beta_{f_+}\right) \end{cases} \tag{2}$$

The identical frequency-independent prefactors in the above expressions are omitted. $\Delta\beta_{f\mp}$ inside sinc functions are the phase-matching terms [27]:

$$\begin{cases} \Delta\beta_{f_-} = \beta_V^{\omega_p} - \beta_H^{\omega_s} - \beta_V^{\omega_i} - \dfrac{2\pi}{\Lambda} \\ \Delta\beta_{f_+} = \beta_V^{\omega_p} - \beta_H^{\omega_i} - \beta_V^{\omega_s} - \dfrac{2\pi}{\Lambda} \end{cases} \tag{3}$$

Subscripts p, s and i denote pump, signal and idler respectively. β_H^{ω} (β_V^{ω}) is the waveguide propagation constant for the H(V) polarization at angular frequency ω, Λ is the QPM period, and L is the length of the nonlinear medium. If QPM is not used, the last term in Eq. (3) is dropped, which does not affect the subsequent discussions.

To reveal the role of dispersion, we expand β_H^{ω} and β_V^{ω} in Eq. (3). Assuming QPM is achieved at ω_o=$\omega_p/2$, energy conservation leads to $\Delta\omega_s = -\Delta\omega_i = \omega_s - \omega_o$. Keeping the first and second order terms, Eq. (3) becomes:

$$\Delta\beta_{f\mp}(\Delta\omega_s) = \mp M \times \Delta\omega_s + \beta_2 \times \Delta\omega_s^2 \tag{4}$$

where

$$M = v_{gV}^{-1}(\omega_o) - v_{gH}^{-1}(\omega_o) \tag{5}$$

$$\beta_2 \approx \frac{1}{2}\left(\frac{\mathrm{d}^2\beta_H}{\mathrm{d}\omega^2} + \frac{\mathrm{d}^2\beta_V}{\mathrm{d}\omega^2}\right)\Bigg|_{\omega=\omega_0} \tag{6}$$

The phase-matching bandwidth is determined by the frequency $\Delta\omega_s$ range where $\mathrm{sinc}^2\left[\frac{1}{2}\Delta\beta(\Delta\omega_s)L)\right] \geq 0.5$. Eq. (4) shows that phase-matching bandwidth is mainly limited by two factors: the second-order chromatic dispersion β_2, which we call dispersion, and M, which we call group birefringence, as it is proportional to the group index difference between the two orthogonally polarized modes.

Let us first consider the case when phase-matching bandwidth is limited by group birefringence, i.e. $|M\Delta\omega_s| \gg |\beta_2\Delta\omega_s^2|$ over the phase-matching bandwidth. Let x_o be the positive solution of $\mathrm{sinc}^2(x)$=0.5, then the condition for the group-birefringence-limited case can be equivalently written as $|M| \gg (2|\beta_2|x_o/L)^{1/2}$. By omitting the second order term, the f_+ and f_- functions

Optics EXPRESS

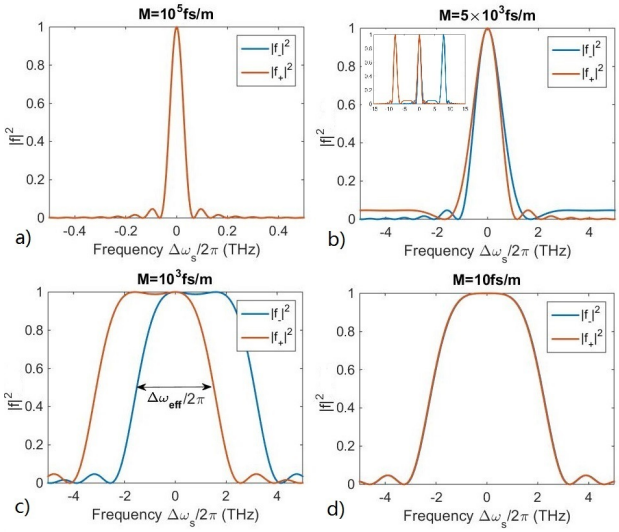

Fig. 1. Illustration of $|f_-|^2$ and $|f_+|^2$ with β_2=100fs^2/mm, L=0.15m, and M = (a) 10^5fs/m, (b) 5×10^3fs/m, (c) 10^3fs/m, and (d)10fs/m. The inset of (b) uses an expanded frequency axis to show that phase matching is also achieved at side peaks. However the biphotons generated there are spectrally distinguishable.

become:

$$f_{\mp}(\Delta\omega_s) \sim \exp\left(\mp\frac{i}{2}ML\times\Delta\omega_s\right)\mathrm{sinc}\left(\mp\frac{1}{2}ML\times\Delta\omega_s\right) \tag{7}$$

where $M\times L$ is the overall differential group delay. In this case the spectral amplitude will be identical, i.e. $|f_-|^2$=$|f_+|^2$, which means spectrum will not provide any polarization information. An example of which is illustrated in Fig. 1(a). However, due to the phase difference between f_- and f_+, temporal distinguishability will be revealed by inverse Fourier Transform (iFT) of Eq. (7) into the time domain [28]:

$$f_{\mp}(\Delta\omega_s) \xrightarrow{iFT} \tilde{f}_{\mp}(t) \propto \mathrm{rect}\left[\frac{1}{ML}(t\mp\frac{ML}{2})\right]. \tag{8}$$

In Eq. (8) we see that the temporal walk-off ML also happens to be the temporal widths of the functions f_- and f_+. In this limit, the two wavepackets will always be completely distinguishable, and temporal compensation will always be required to eliminate distinguishability. Such is the case for most conventional nonlinear media used for type-II SPDC (see table.1).

Next, let us consider the opposite case, when group birefringence is comparably small, i.e.

$$|M| \ll \sqrt{2|\beta_2|x_o/L}. \tag{9}$$

In this case, $\Delta\beta$ in Eq. (4) is determined by β_2 instead of ML, and $f_{\mp}$ functions become:

$$f_{\mp}(\Delta\omega_s) \sim \exp\left(\mp\frac{i}{2}ML\times\Delta\omega_s\right)\mathrm{sinc}\left(\mp ML\times\Delta\omega_s+\beta_2 L\times\Delta\omega_s^2\right). \tag{10}$$

Optics EXPRESS

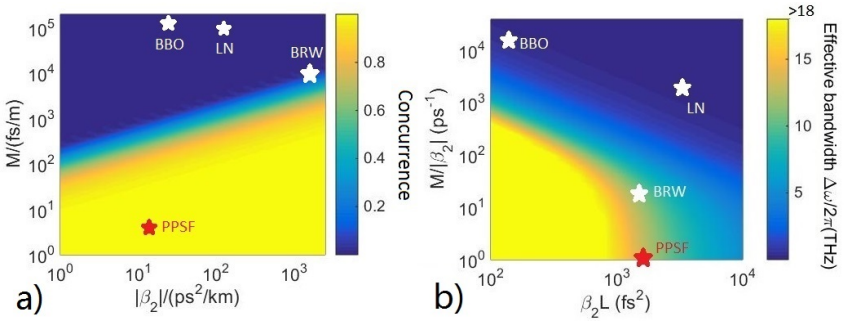

Fig. 2. a) Calculated concurrence (without temporal compensation or spectral filtering) varies with M and dispersion. b) Simulated effective bandwidth over which both high spectral brightness and high spectral industinguishability can be obtained. BBO (β-BaB_2O_2), LN (lithium niobate) and AlGaAs Bragg reflection waveguides (BRWs) are compared with PPSF, using parameters found in Table.1.

Taking $f_{\mp}(\Delta\omega_s)$ to temporal domain by iFT, we have,

$$f_{\mp}(\Delta\omega_s) \xrightarrow{iFT} \tilde{f}_{\mp}(t) \sim F\left[\sqrt{\frac{1}{|\beta_2|L}}(t \mp \frac{ML}{2})\right] \tag{11}$$

where,

$$F(t) = \sqrt{\frac{\pi}{2}}t\left[S\left(\frac{t}{\sqrt{2\pi}}\right) - C\left(\frac{t}{\sqrt{2\pi}}\right)\right] + \sin\left(\frac{t^2}{4}\right) + \cos\left(\frac{t^2}{4}\right) \tag{12}$$

$S(t)$ and $C(t)$ in Eq. (12) are Fresnel S and C integrals. If we examine the $F\left[\sqrt{\frac{1}{|\beta_2|L}}(t \mp \frac{ML}{2})\right]$ function in Eq. (11), we see that the temporal walk-off is $M \times L$ while the temporal width of the function is $\sim (|\beta_2|L)^{1/2}$. Under the condition of Eq.(9), the temporal walk-off is much smaller than the temporal width, i.e., temporal distinguishability is negligible. Equivalently, in spectral domain, the phase difference between f_- and f_+, $\Delta\phi$=$ML\Delta\omega_s$, is nearly constant over the whole generation spectral range (e.g. <0.02 rad in PPSF). Such is the case where the temporal walk-off does not have to be compensated.

We further investigate the spectral distinguishability as a result of M in Eq. (11), as $|f_-|^2$ and $|f_+|^2$ are no longer identical for finite M values. Fig. 1(b) and 1(c) show two numerical examples where $\beta_2\Delta\omega_s^2$ still dominates the phase matching bandwidth, but M is significant enough to cause spectral distinguishability. Fig. 1(d) shows the case where M is so small that spectral distinguishability is essentially eliminated. Such is the case to obtain compensation-free broadband entanglement with high quality of entanglement.

To quantify the overall entanglement quality, we provide simulation results of concurrence C as a function of both group birefringence and dispersion. Concurrence is a convenient measure of bipartite entanglement in its own right [29]. In terms of polarization entanglement, concurrence can be obtained by tracing over the spectral degree freedom of the total density matrix $\rho = |\Psi\rangle\langle\Psi|$, with $|\Psi\rangle$ given in Eq. (1). Combining with the definition of concurrence:

$$\mathrm{C} = \max\{0, \lambda_1 - \lambda_2 - \lambda_3 - \lambda_4\} \tag{13}$$

where λ_i are the eigenvalues in decreasing order of the Hermitian matrix $R = \sqrt{\sqrt{\rho}\tilde{\rho}\sqrt{\rho}}$, we

Optics EXPRESS

Table 1. Comparison between PPSF, a BRW based on AlGaAs, typical nonlinear material LN and BBO, for type-II SPDC generation at λ=1.55μm.

Material	|M| (fs/m)	$\|\beta_2\|$ (fs^2/mm)	L (mm)	$\frac{\|M\|}{\sqrt{2\|\beta_2\|x_o/L}}$
PPSF (this work)	<10	15	185	<0.02
BRW [30,31]	2.33×10^4	~1100	1.9	~0.6
LN [32,33]	2.7×10^5	~100	36	~52
BBO [28,34]	3.8×10^5	~30	5.6	~134

obtain [26]:

$$C = \left| \int \mathrm{d}\omega_s \int \mathrm{d}\omega_i \; f_-(\omega_s,\omega_i) f_+(\omega_s,\omega_i)^* \right|. \tag{14}$$

Figure 2(a) shows the simulated concurrence using the approximation expressed by Eq. (4). It can be seen that, to maintain high concurrence without compensation, low group birefringence is a must. Moreover, higher dispersion can also ease the requirement for low group birefringence in order to obtain high concurrence.

Next, we briefly discuss the impact of group birefringence and dispersion on bandwidth of the type-II SPDC source. When group birefringence dominates, according to Eq. (7) the FWHM bandwidth is simply $\Delta\omega$=$4x_o/ML$. To broaden the bandwidth, M or L should be reduced. When dispersion dominates, however, the bandwidth consideration is more subtle. Because in this case the group birefringence leads to spectral distinguishability and therefore affects the bandwidth over which high concurrence can be obtained (as opposed to the bandwidth of high spectral brightness). The FWHM bandwidth of spectral brightness based on Eqs. (2) and (4) is:

$$\Delta\omega_{|f^{\mp}|^2} \approx \sqrt{\left(\frac{M}{\beta_2}\right)^2 + \frac{8x_0}{L|\beta_2|}}. \tag{15}$$

If we consider the spectral range with both high brightness and high spectral overlap, then the *effective* bandwidth (for example, see Fig. 1c) can be approximated by:

$$\Delta\omega_{\mathrm{eff}} \approx \Delta\omega_{|f^{\mp}|^2} - \left|\frac{M}{\beta_2}\right|. \tag{16}$$

Equation (16) indicates that the bandwidth reduction due to spectral distinguishability is propotional to $|M/\beta_2|$. In other words, spectral indistinguishablity requires that $\left|M/\beta_2\right| \ll (8x_o/L|\beta_2|)^{1/2}$, which is consistent with the condition of Eq. (9). The effective bandwidth versus $|M/\beta_2|$ and $|\beta_2|L$ is plotted in Fig. 2b for both nonlinear crystals/waveguides and PPSF. We can see that both lowering the group-birefringence-to-dispersion ratio ($|M/\beta_2|$) and lowering $|\beta_2|$ can lead to broader bandwidth. The former is also better for concurrence, while the latter is not.

In summary, the low group birefringence condition expressed in Eq. (9) ensures both spectral and temporal indistinguishability without the need for compensation. It also leads to high spectral brightness over a large bandwidth. Therefore, Eq. (9) is what is required for broadband polarization-entanglement generation via type-II SPDC without compensation. PPSF clear demonstrates its superiority in meeting this requirement.

3. Simulation and experiment on PPSF

In this section, we show through simulation (based on fiber geometries and material properties) and experiment that broadband polarization-entanglement can indeed be achieved in PPSF with

Optics EXPRESS

high quality of entanglement.

The PPSF we use has a cross-section geometry similar to that of [35], with two air holes on either side of the core. The fiber has an NA≈0.20 (at λ=1.55 μm). The air hole radius is 21.5 μm, and one of them is intentionally placed closer to the core to optimize second order nonlinearity through thermal poling. The $|\beta_2|$ for this geometry is ~15fs^2/mm, which basically depends on the dispersion of core material. We can also tune the M value by changing the eccentricity of the core and/or the two air-hole distances, which allows us to design the PPSF for a specific output spectrum, or to match the simulation with experimental results.

In our simulation, stress-induced index change is ignored, as stress is mostly relieved during the fiber draw. Sellmeier equations of air, fused silica and Germanium-doped fused silica are taken from [36–38] to ensure the accuracy of material dispersion modeling. A finite element eigenmode solver (Lumerical) is used for calculating dispersion and group birefringence of the fiber modes. The normalized spectral brightness $|f_{\mp}|^2$ can then be obtained from Eq. (2) for a given pump frequency. To simulate the experimental cases where a long pump pulse is used, we linearly sum up the spectral brightness produced by a finite number of pump frequencies over the pump spectral range, assumed to be Gaussian with a FWHM bandwidth of ~0.2nm.

Two PPSF samples were used experimentally. One has a periodically-poled section of 17 cm and a measured M value of ~50fs/m, and the other has a periodically-poled length of 18.5cm, but the M value of this sample is smaller than our measurement sensitivity in the range of 1510-1590nm, which is ~10fs/m. Fitting to experimental spectrum results in an estimated $M \approx$ 8fs/m. The spectral intensity of the two functions $|f_{\mp}|^2$ are measured dispersively using a fiber spectrometer [39], where the biphoton spectral information is mapped onto the temporal domain by passing through 20 km of SMF-28 fiber. Given the detector temporal resolution of 180ps, the spectral resolution of our measurement is 0.5nm. The overall $|f_{\mp}|^2$ spectrum is stitched together due to the limitation of the fiber spectrometer. More experimental details and methodology can be found in [39].

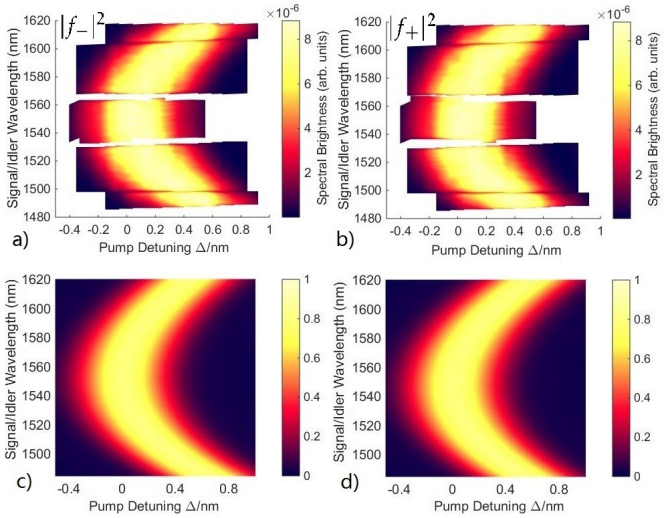

Fig. 3. a) and b) Experimental tuning curves of $|f_-|^2$ and $|f_+|^2$ are obtained from the PPSF sample with M≈50fs/m and L≈17cm, measured using various filter sets. c) and d) The simulated tuning curves of $|f_-|^2$ and $|f_+|^2$.

Figure 3 demonstrates the good agreement between experimental and simulated tuning curves. Figure 3 (a) and (b) are amalgamations of measured $|f_{\mp}|^2$ at different pump detuning wavelengths, $\Delta \equiv \lambda_p - 2\lambda_o$, where $\lambda_o = c/2\pi\omega_o$ is defined by the QPM period.

Optics EXPRESS

Figure 4 shows the essentially identical $|f_-|^2$ and $|f_+|^2$ spectra measured in a PPSF sample with M<10fs/m, compared with the simulated $|f_\mp|^2$ functions assuming a M value of 8fs/m. The concurrence calculated from the $f_\mp$ functions using Eq. (14) integrated over the entire bandwidth is >0.995. Such compensation-free high concurrence would not be possible using a nonlinear crystal or waveguide.

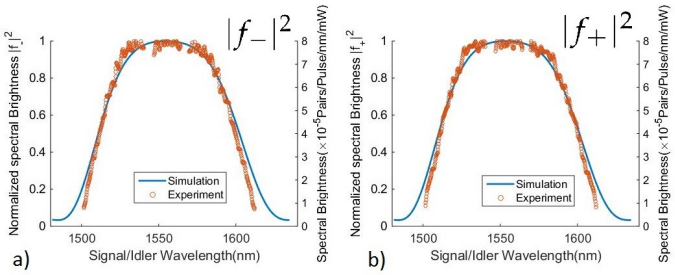

Fig. 4. Simulated and experimental spectral brightness results of the second PPSF sample with M ≈8fs/m and L≈18.5cm at Δ≈0nm. a) $|f_-|^2$, b) $|f_+|^2$. The tail of the experimental spectral brightness is a little bit off due to the filter cutoff effect

In some applications of broadband polarization-entangled sources, entanglement is distributed to many users through narrow spectral filtering of the signal and idler photons [12, 13], similar to the wavelength demultiplexing in classical optical communications. We note in such cases, the quality of entanglement can be improved by filtering. Intuitively, filtering corresponds to widening the biphoton temporal width, making the temporal indistinguishability even less significant. Interpreted in the spectral domain, filtering reduces the spectral distinguishability within the filter bandwidth for most parts of the usable spectral range of the source. If the filter bandwidth is sufficiently narrow that the f_- and f_+ functions are essentially not varying over the filter bandwidth, then we can do away with the frequency integrals and define a filtered concurrence

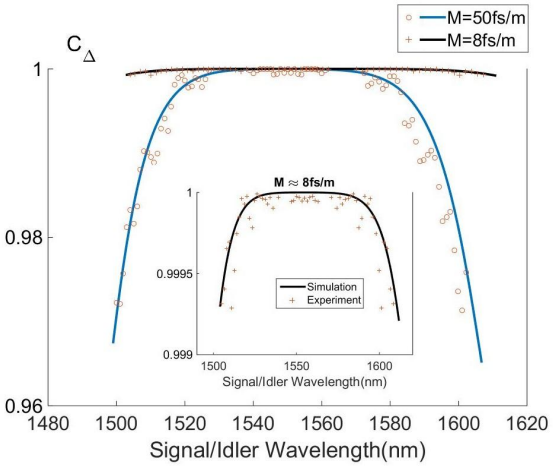

Fig. 5. C_Δ calculated from experimentally measured $|f_\mp|^2$ functions (red dots and red cross) and from simulation (blue line and black line) for two of our PPSF samples with M ≈50fs/m and M ≈8fs/m respectively at zero detuning according to Eq. (17). The inset shows the detailed curve of the sample with M ≈8fs/m.

Optics EXPRESS

C_Δ to quantify the quality of entanglement after filtering:

$$C_\Delta(\omega_s,\omega_i)=\frac{|2f_-(\omega_s,\omega_i)f_+^*(\omega_s,\omega_i)|}{|f_-(\omega_s,\omega_i)|^2+|f_+(\omega_s,\omega_i)|^2}. \tag{17}$$

Figure 5 shows the C_Δ calculated from experimentally measured $|f_\mp|^2$ functions and that from simulation, for both fiber samples. It can be seen that a lower M value dramatically increases the entanglement quality under the same experimental conditions, from C_Δ>0.96 for M~50fs/m to C_Δ>0.999 for M <10fs/m, over 100nm bandwidth.

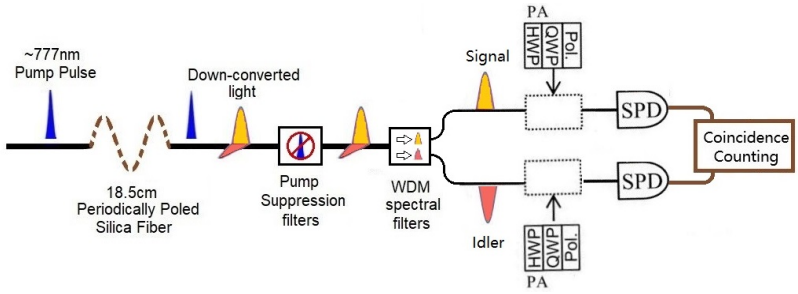

Fig. 6. Experimental setup: The PPSF is pumped by a Ti:Sapph source (not shown). WDMs spectrally separate the down-converted photons, which are then detected by a pair of single-photon detectors (SPDs). The coincidence counts are recorded by a digital circuit. Polarization analyzers (PAs) are added to demonstrate polarization entanglement. Each PA consists of an achromatic half- (HWP) and quarter-wave plate (QWP) and a polarizer (Pol)

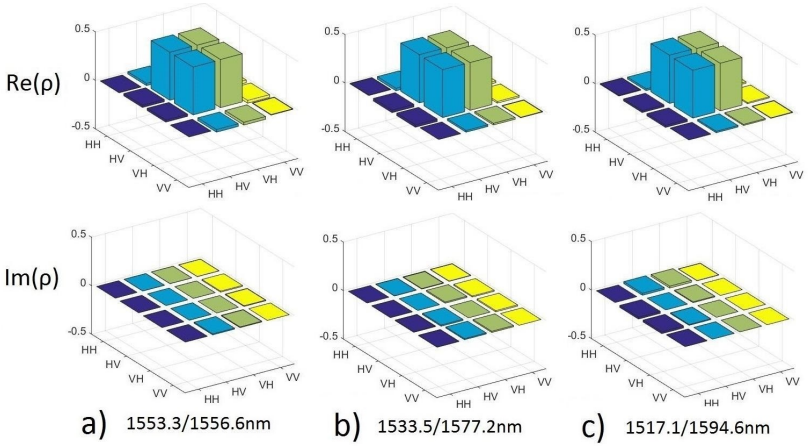

Fig. 7. Density matries ρ reconstructed from experimental quantum-state tomography (without accidental subtraction) using three 1.3nm passband filter sets centered at λ_s/λ_i= a) 1553.3/1556.6nm, b) 1533.5/1577.2nm, c) 1517.1/1594.6nm. Concurrence and Fidelities results are given in Table.2.

Quantum state tomography (QST) measurements are demonstrated on biphotons generated in the M ≈8fs/m sample using experimental setup shown in Fig. 6. A mode-locked (81.6 MHz, 400 ps pulsewidth) Ti:Sapph laser [not shown in Fig. 6] is used as the pump. A pump suppression filters reducing the pump power by >110 dB is used at the end of the 18.5cm PPSF (M<10fs/m), followed by filters to seperate signal and idler photons. To demonstrate QST at different conjugated

Optics EXPRESS

wavelength pairs, three different filter sets (wavelengthes are shown in Fig. 7) are used respectively. The total loss, including the efficiency of the free-runing single photon detectors (ID Quantique id220, 20μs deadtime) is estimated ~16dB. The 4000 pairs/25s generation rate at a external pump power of ~13mW corresponds to a generation rate of 1.4×10^4pairs/s/nm/mW, along with single photon counts of $\sim10^4$ counts/25s at each of the single photon detectors. The total generation rate over the whole spectral range is estimated to be $\sim1.4\times10^6$pairs/s/mW. Measurement by QST (Fig. 7) resulted in a filtered concurrence of 0.977 ± 0.005 (0.993 ± 0.005 after accidental subtraction), and a filtered fidelity to $|\Psi^+\rangle$ of 0.987 ± 0.005 over at least 77nm bandwidth, the highest concurrence reported for a compensation-free type-II SPDC source. Measurement results are given in Table.2.

The largest spectral separation between signal and idler photons that we have tested (77nm) is limited by the conjugated filter pairs available to us. The entangled photon source itself provides larger bandwidth as shown in Fig. 5. The narrowband filters (transmission bandwidth ~1.3nm) we used made the measurements more susceptible to slight pump wavelength deviations, which can lead to degradation in concurrence or fidelity. Pump detuning is chosen to be $\Delta \approx 0$ nm to match the filter pairs. With filters of suitable wavelengths and a slightly positive pump detuning as illustrated in Fig. 3, for example, $\Delta \approx +0.25$nm in [25], polarization-entangled biphotons with broader spectrum and higher entanglement quality can be obtained.

In addition, the spectral brightness of PPSF with the M<10fs/m presented in this paper is ~10× higher than the previous PPSF [24, 25] because of the enhancement in poling technique. The spectral brightness and total brightness of PPSF source is comparable to other nonlinear crystal or waveguide based SPDC broadband polarization entanglement sources [13, 23, 40], but provide better entanglement quality. Even though the $\chi^{(2)}$ in PPSF ($\chi^{(2)}_{\text{eff}} \sim 0.09pm/V$) is one or two orders of magnitude lower than nonlinear crystals [13, 41] (~1-30pm/V), PPSF can offer one or two orders of magnitudes longer nonlinear interaction length, while the SPDC emission brightness is propotional to $(\chi^{(2)}L)^2$. Besides, PPSF source can take advantage of its very low noise. Unlike other nonlinear crystals or waveguide based sources where there is a significant trade-off between brightness and visibility, we can always achieve high brightness by pumping harder as long as the probability of multi-pair emission is kept low.

Lastly, we show the two photon interference (TPI) results at three different sets of conjugated wavelengths in Fig. 8. The visibilities for all the basis measured are found to exceed 98.4% for all three frequency-conjugate sets without subtracting the background. Both QST and TPI results demonstrated high quality broadband polarization entanglement, as a result of the extremely low group birefringence of the fiber sample.

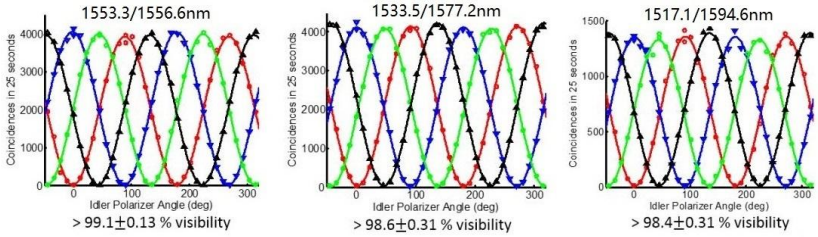

Fig. 8. Two photon interference results for the three frequency-conjugate pairs with bandwidth ~ 1.3nm. Red dots: H basis; Blue dots: V basis; Green dots: A basis; Black dots: D basis. Visibility values are obtained without subtraction of accidentals.

Optics EXPRESS

Table 2. QST and TPI experiment results of the 18.5cm, M<10fs/m PPSF sample using three different sets of filters without accidental subtraction. Concurrence are calculated from Eq. (13). Fidelity is calculated by $F = \langle\Psi^+|\,\rho\,|\Psi^+\rangle$, where $|\Psi^+\rangle = \frac{1}{\sqrt{2}}(|HV\rangle + |VH\rangle)$. After subtraction of accidentals, all concurrence and fidelities are >0.99.

Filter set	1553.3/1556.6nm	1533.5/1577.2nm	1517.1/1594.6nm
Concurrence C	0.988±0.002	0.985±0.002	0.977±0.005
Fidelity to $\|\Psi^+\rangle$	0.989±0.002	0.989±0.002	0.987±0.005
Visibility of TPI	>99.1±0.13%	>98.6±0.31%	>98.4±0.31%

4. Conclusion

Based on theoretical derivation of type-II SPDC, we have shown how group birefringence leads to both temporal and spectral distinguishability, the degree of which depends intricately on the dispersion of the nonlinear medium. We further showed that broadband polarization entanglement from type-II SPDC can be obtained *without compensation* if condition Eq. (9) is met. The performance enhancement resulting from lowering group birefringence will benefit many quantum applications. For example, a broader bandwidth leads to better resolution in quantum optical coherence tomography [42]. Higher entanglement quality over a broad range enables higher dimentional QKD [12, 13] without increasing the bit error rate at side channels. The generated broadband biphotons with near constant phase might further benefit applications in frequency domain quantum information processing [43].

Experimentally, condition Eq. (9) cannot generally be achieved in nonlinear crystals or waveguides, but can be readily achieved in PPSF. In such a fiber, the group birefringence can essentially be reduced to zero through appropriate fiber design, resulting in a dispersion-limited bandwidth, and high quality polarization entanglement can be obtained over the entire bandwidth. Given that the dispersion in fiber can also be tailored easily, the bandwidth of such a source can be designed to be very wide. We experimentally demonstrated very high concurrence values (>0.99) over more than 77nm bandwidth with PPSF. By comparing the entanglement quality using a fiber spectrometer under the same condition, we demonstrated that lower group birefringence will dramatically increase the entanglement quality in a compensation-free scheme. The bandwidth of PPSF source can be further broadened without losing entanglement quality if suitable pump wavelength are applied and the group velocity dispersion of the fiber are engineered.

Funding

Natural Sciences and Engineering Research Council of Canada (RGPIN-2014-06425, RGPAS 462021-2014); Applied Basic Research Program of Wuhan (2017010201010102).

Acknowledgment

The authors would like to thank Dr. Franco N.C. Wong for helpful discussions.